ACS OMEGA

http://pubs.acs.org/journal/acsodf

Article

Strain Effects on the Two-Dimensional Cr_2N MXene: An Ab Initio Study

Sandra Julieta Gutiérrez-Ojeda,* Rodrigo Ponce-Pérez, Daniel Maldonado-Lopez, Do Minh Hoat, Jonathan Guerrero-Sánchez, and Ma. Guadalupe Moreno-Armenta*

Cite This: *ACS Omega* 2022, 7, 33884−33894

Read Online

ACCESS | Metrics & More | Article Recommendations | Supporting Information

ABSTRACT: Structural, electronic, and magnetic properties of two-dimensional Cr_2N MXene under strain were studied. The uniaxial and biaxial strain was considered from −5 to 5%. Phonon dispersion was calculated; imaginary frequency was not found for both kinds of strain. Phonon density of states displays an interesting relation between strain and optical phonon gaps (OPGs), that it implies tunable thermal conductivity. When we apply biaxial tensile strain, the OPG increases; however, this is not appreciable under uniaxial strain. The electronic properties of the dynamically stable systems were investigated by calculating the band structure and electron localization function (ELF) along the (110) plane. The band structure showed a metallic behavior under compressive strain; nevertheless, under tensile strain, the system has a little indirect band gap of 0.16 eV. By analyzing, the ELF interactions between Cr−N are determined to be a weaker covalent bonding Cr_2N under tensile strain. On the other hand, if the Cr atoms reduce or increase their self-distance, the magnetization alignment changes, also the magnetic anisotropy energy displays out-of-plane spin alignment. These properties extend the potential applications of Cr_2N in the spintronic area as long as they can be grown on substrates with high lattice mismatch, conserving their magnetic properties.

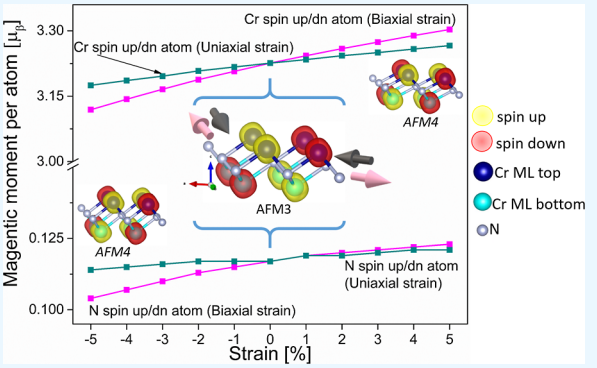

INTRODUCTION

Spintronics is one of the most active research fields. Contrasting conventional electronic devices which are performed by a charge carrier, the switch of a spin-governed device uses spin waves as information carriers or by the magnon−phonon effect, which can be much faster and with less power dissipation.[1−3]

Since the remarkable physical and chemical properties of graphene were explored,[4,5] other two-dimensional (2D) materials have attracted interest and attention because of their intrinsic properties[6−9] that are being actively sought to fabricate high-performance electronic devices. A great solution to reduce inefficiencies of graphene and quasi-graphene structures is the creation of graphene-based van der Waals (VdW) heterostructures by positioning graphene on top of other 2D materials.[10]

In spite of the research efforts in 2D semiconductors and optoelectronics materials, 2D magnetic materials remain still unexplored, due to the fact that most of the 2D materials already synthesized have been intrinsically nonmagnetic. However, experimental and theoretical studies in recent years reveal that magnetic properties can be controlled by introducing edge structures, doping, surface functionalization, or creating defects.[11−13] In this sense, 2D hexagonal CrN displays half-metal behavior with a possible ferromagnetic (FM) ordering when it is isolated[14] and preserves its properties as it happens in $MoSe_2$ and MoS_2 heterostructure.[15] Besides, strain engineering[16] is an important strategy for tuning the lattice and electronic structure of 2D materials, and there are different methods of inducing strain from the lattice mismatch, for example, the use of different substrates, such as flexible substrates, patterned substrates, and piezoelectric substrates, to the action of atomic force microscope tips and bubbles.[17]

MXenes are a new family of 2D transition-metal carbide/nitrides, discovered in 2011,[18] which are a family of layered hexagonal transition-metal carbides/nitrides with theoretically infinite lateral dimensions but atomically thin thickness.[19] The chemical formula is $M_{n+1}X_nT_2$ (n = 1, 2, and 3), where M is an early transition-metal element, X is carbon or nitrogen, and T (T = OH, O, and F) is a surface functional group.[20] Since the first discovered $Ti_3C_2T_2$ MXene, more than 70% of all MXene research has been focused on it.[21] MXenes had been predicted, and their physics and chemical properties were described by

Received: May 4, 2022
Accepted: August 4, 2022
Published: September 13, 2022

https://doi.org/10.1021/acsomega.2c02751
ACS Omega 2022, 7, 33884−33894

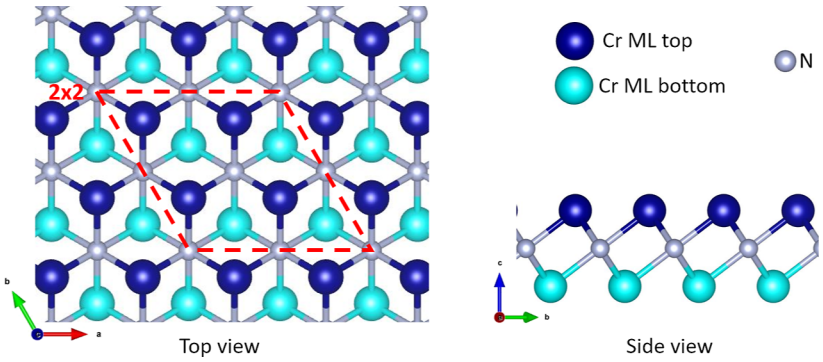

Figure 1. Top and side view of Cr2N MXene with (2 × 2) periodicity.

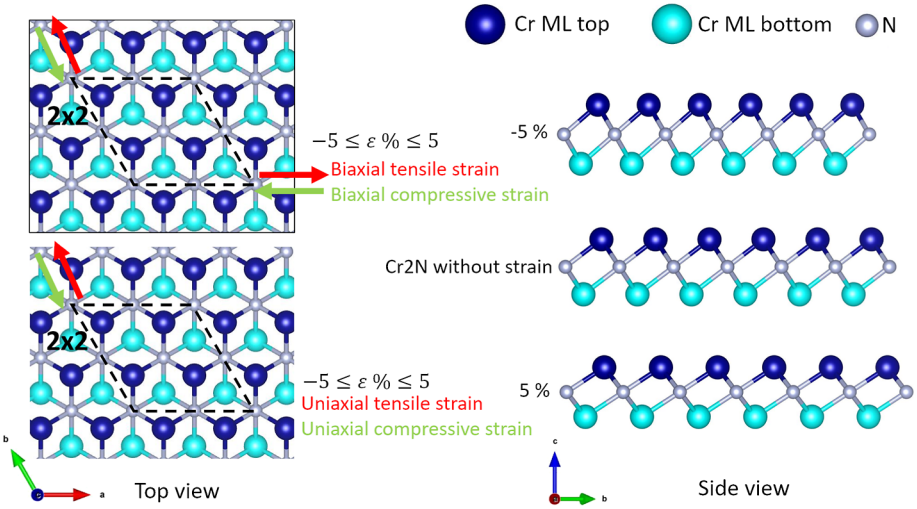

Figure 2. Top and side view of Cr_2N under biaxial and uniaxial strain.

theoretical studies,[22] principally with intrinsic ferromagnetism.[23−25] The MXenes exhibit outstanding electronic, optical-mechanical, and thermal properties with versatile transition metal and surface chemistries.[26] Furthermore, they could be a promising candidate to be employed in heterostructures as metal electrodes, photodetectors, and in solar cell applications,[27−29] and due to the VdW interactions, they can be candidates for anodes in batteries.[30] In addition, when strain is applied on MXenes, for example $WCrCO_2$, their electronic properties change to a semi metallic character with a dual narrow band gap.[31] The VdW heterostructure Mn_2CFCl/MoSSe has the potential applications in spintronic devices due to its perpendicular magnetic anisotropy (PMA) that can be regulated by the biaxial strain and an external electric field.[32]

The nitride-based MXene possess an advantage in comparison with carbide MXenes due to a higher electronic conductivity[30,33] and magnetic moments,[34] so they could be suitable candidates for electrodes in electrochemical capacitors or metamaterials devices.[35,36] Moreover, a previous theoretical study had considered possible magnetic configurations where the most favorable for Cr_2N pristine is the antiferromagnetic (AFM) order where the different Cr layers are antiparallel to each other and have metallic behavior.[37] Nevertheless, this MXene displays a FM ground state that acts a half-metallic when it is functionalized,[34,37] also the ground state above room temperature is stable, robust, and can be maintained under tensile strains up to 10%.[38] Subsequently, the electronic and magnetic properties could be tunable by applying compressive and tensile strain, such is the case for the MXene semiconductors[34] and in the MXenes that display magnetic anisotropy.[39]

Electronic and magnetic properties of Cr_2N MXene could be tunable as a result of lattice parameter mismatch to build heterostructure or by deformation induction, as shown in 2D systems.[39,40] In this sense, we study the biaxial and uniaxial strain effect on Cr_2N MXene pristine. The MXene is dynamically stable under compressive or tensile stress and keeps its metallic characteristics. Even if it preserves the AFM behavior, the magnetic spin polarization between Cr layers is different to pristine MXene unstrained, and the magnetic moment magnitude depends if it is under compressive or tensile strain, allowing it to be a good option for applications in 2D spintronics as contacts.

COMPUTATIONAL METHODS

The structural, electronic, and magnetic properties of the Cr_2N MXene under tensile and compressive strain are investigated by spin-polarized first-principle calculations. Calculations were performed in the periodic density functional theory (DFT) framework, as implemented in the Vienna Ab initio Simulation Package,[41−43] that utilizes a plane wave basis set to represent electron states. The exchange−correlation energies were treated using the generalized gradient approximation with Perdew−Burke−Ernzerhof parametrization.[44] Because Cr is a transition metal with 3d orbitals, it exhibits high correlation electrons. Therefore, to treat the high correlated electrons, we

https://doi.org/10.1021/acsomega.2c02751
ACS Omega 2022, 7, 33884−33894

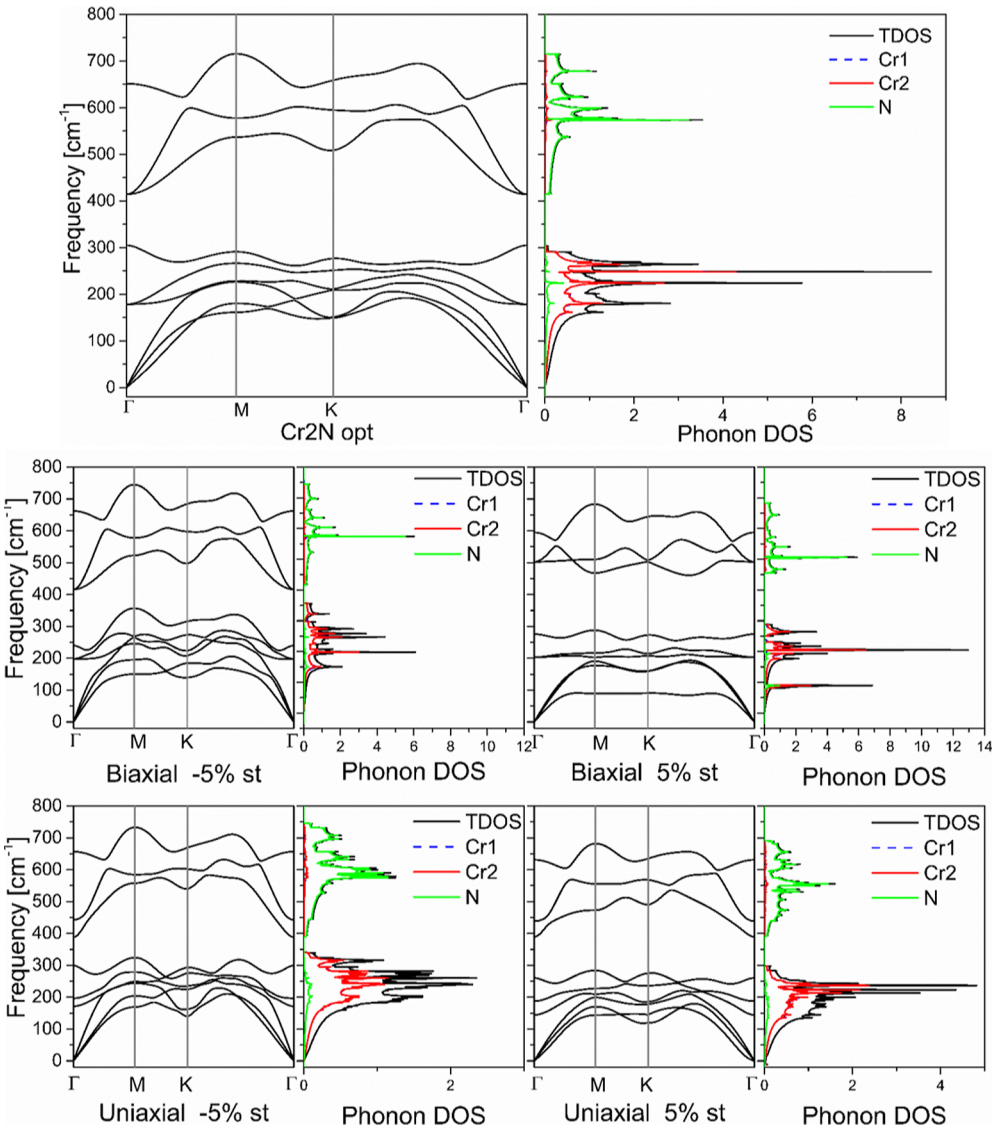

Figure 3. Phonon band structure and densities of states of unstrained Cr_2N (upper part), under biaxial compressive and tensile strain (middle part), and under uniaxial compressive and tensile strain (bottom part).

use the Hubbard Correction (DFT + U) method,[45] employing the methodology proposed by Dudarev et al.[46] We employed a value of U = 3 eV to treat the Cr-3d orbitals as in previous reports.[47] The electronic states were expanded using the projector-augmented wave basis[48,49] with an energy cutoff of 460 eV. The Cr_2N MXenes were simulated with the supercell method with a vacuum space of 15 Å. To study the electronic and magnetic properties, a monolayer of the Cr_2N supercell with 2 × 2 periodicity was constructed, and we consider different magnetic configurations without any constraints. To achieve convergence, all the force components must be less than 0.01 eV/Å and total energy differences less than 1×10^{-9} eV. The Brillouin zone was sampled using a Monkhorst−Pack mesh[50] of 15 × 15 × 1 k points. Phonon dispersions were obtained using the finite-differences method[51] combined with the Phonopy code.[52] By using 2 × 2 periodicity with integration of 7 × 7 × 1, the dynamical stability of the system has been achieved. Furthermore, the molecular dynamics simulations were performed by the CASTEP package[53] at 300 K, and a time step of 5 fs is set with 500 simulation steps.

RESULTS AND DISCUSSION

The structure of MXene was built by removing the A-element group element atomic layer from their corresponding Cr_2GaN MAX phase (mostly IIIA and IVA).[47,54] The unit cell includes three atoms, two chromium (Cr) and one nitrogen (N), which resides in the $P\bar{3}m1$ space group. The Cr atoms are located at (1/3, 2/3, z) and (2/3, 1/3, −z) on the 2d Wyckoff sites; meanwhile, the N atom is located at (0, 0, 0) on the 1a Wyckoff site.[5556] Then, the MXene Cr_2N has a centered honeycomb (T) structure where the N atoms are in-between two layers of the hexagonal lattice of Cr atoms.[57] The interplanar distance is 1.14 Å, and the Cr−N bonds have a distance of 2.12 and 2.06 Å, for more details see Figure S1 in Supporting Information. Figure 1 displays a top and side view of the crystal structure of the unstrained Cr_2N MXene.

To study the strain effect on this MXene, biaxial (x−y) and uniaxial (y) strain (ε) was applied, see Figure 2. The strain is defined as

https://doi.org/10.1021/acsomega.2c02751
ACS Omega 2022, 7, 33884−33894

Table 1. Vibrational Mode Frequencies of the Stable Cr_2N MXene[a]

	Raman modes			IR modes		
$P\bar{3}m1$ (164)	E_g		A_{1g}	A_{2u}		E_u
Cr_2N unstrained	179.28		305.14	416.17		651.67
−5% biaxial strain	198.49		239.75	416.36		661.91
5% biaxial strain	203.61		275.72	594.77		502.81
−5% uniaxial strain	171.65	196.66	299.23	388.51	442.84	656.68
5% uniaxial strain	144.36	187.79	260.26	389.65	438.78	631.05

[a]E modes are degenerate.

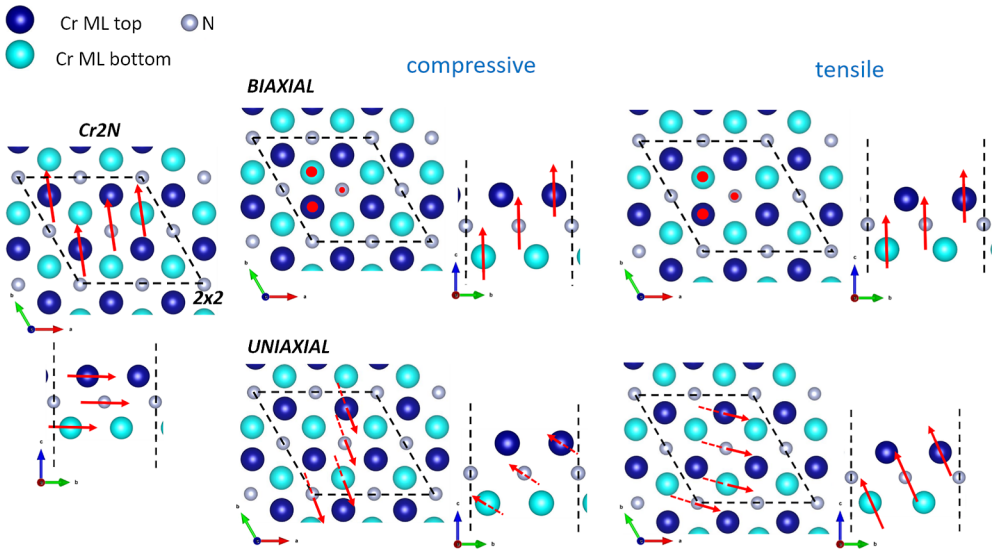

Figure 4. Atomic displacements of the vibration modes for Cr_2N MXene unstrained and under biaxial or uniaxial compressive and tensile strain. The dot on the atom corresponds to vibration direction pointing into the plane, and the arrow corresponds to the in-plane vibration.

$$\varepsilon = \frac{(a - a_0)}{a_0} = \frac{\Delta a}{a_0} \times 100\% \quad (1)$$

where a_0 and a are the lattice parameters of the unstrained and strained structures, respectively. The positive and negative values correspond to tensile and compressive strains, respectively, for a range from $-5\% \leq \varepsilon \leq 5\%$ for each deformation.

To determine the dynamical stability, we calculate the phonon bands; results are shown in Figure 3. These phonon dispersions are plotted along the path Γ-M-K-Γ. It is worth to notice that non-negative frequencies are present for any deformation, meaning that the system is stable under biaxial and uniaxial strain in all the range applied. As reported for a similar crystal structure and chemical bonding M_2C MXene,[58] the phonon dispersions have three acoustic modes; two of them exhibit a linear dispersion near Γ and correspond to in-plane rigid body motions. In contrast, the third acoustic mode corresponds to out-of-plane vibrations, and it has a quadratic dispersion close to Γ and lower energy in the rest of the spectrum, which is a common feature in covalent, VdW monolayer and multilayer 2D lattices[55,59,60] due to accuracy of the harmonic interatomic force constants.[61−63] Taking into account the crystal structure of the MXene, the optical modes at the zone center of the Brillouin zone can be classified with the following irreducible formula[64]

$$\Gamma(Cr_2N) = E_g + A_{1g} + A_{2u} + E_u \quad (2)$$

where the E-symmetry modes (E_g and E_u) are doubly degenerate. The two Raman-(E_g + A_{1g}) and IR (A_{2u} + E_u) optical mode frequencies of MXene free and under stress or strained are listed in Table 1. Note that for uniaxial compressive and tensile strain, the E_g and A_{2u} phonon bands unfold, 196.66 and 187.79 cm^{-1} for E_g while for A_{u2} are 442.84 and 438.78 cm^{-1}, see Figure 3. This is due to the symmetry breaking, although the system is dynamically stable, as reported in similar MXenes.[64] The correspondence between the vibrational modes of Cr_2N free and under compressive and tensile strain is determined by the direction of the vibrations and the nature of the contributing atoms, then for Cr atoms, the Raman-active modes are associated with in-plane and out-plane vibrations for E_g and A_{1g}, respectively, as reported by Champagne.[55] The schematic displaced representations of the atoms are illustrated in Figure 4, where the atoms are displaced along $x-y$ for Cr_2N free-strain due to E_g intensity being higher than A_{1g}, while under biaxial and uniaxial strain, the atoms change their out-plane z displacement because the phonon band intensity of A_{1g} is comparable with E_g.

The highest peaks in energy in the phonon density of states (phonon DOS) correspond to N atom vibrations. Moreover, the first three optical branches in the phonon spectrum demonstrate lower frequencies close to the three acoustic phonon branches where it corresponds to the vibration of Cr atoms. Furthermore, the optical phonon gap (OPG) induced is summarized in Table 2. It is noteworthy that under uniaxial strain, the OPG decreases while under biaxial strain decreases and increases when applying compressive and tensile strain,

https://doi.org/10.1021/acsomega.2c02751
ACS Omega 2022, 7, 33884−33894

Table 2. Optical Phonon Gap and Upper Limit Optical Branch for Cr_2N Unstrained and under Strain

		biaxial strain		uniaxial strain	
	Cr_2N unstrained	−5%	5%	−5%	5%
optical phonon gap [cm^{-1}]	109.08	59.38	167.79	48.20	91.23
upper limit optical branches [cm^{-1}]	715.86	744.88	683.67	745.88	656.31

respectively (for details, see Figures S2 and S3 in the Supporting Information). The existence of a phonon gap between optical phonons implies larger thermal conductivity[59] that could be engineered by strain.

In addition, Table 2 exhibits the maximum frequencies of the phonon spectrum that could be associated with the Debye temperature and describe the Debye stiffness of the system[59] due to the fact that it includes the optical phonon excitation resistance.[65] In this sense, Debye stiffness (being an important parameter to represent the resistance to overall phonon excitation[65]) of the Cr_2N under strain is much lower than that of graphene, where the maximum optical frequency is around 1500 cm^{-1},[59] two times higher than the strained Cr_2N MXene.

To analyze the thermal stability of unstrained and strained Cr_2N monolayer, Figure 5 displays the ab initio molecular dynamics (AIMD) simulation results that have been carried out at 300 K. Herein, a time step of 5 fs is set with 500 simulation steps (total simulation time of 2.5 ps). Note that no structural destruction occurs despite its constituent atoms vibrate around their equilibrium positions, suggesting good thermal stability of the studied 2D materials in both unstrained and strained states.

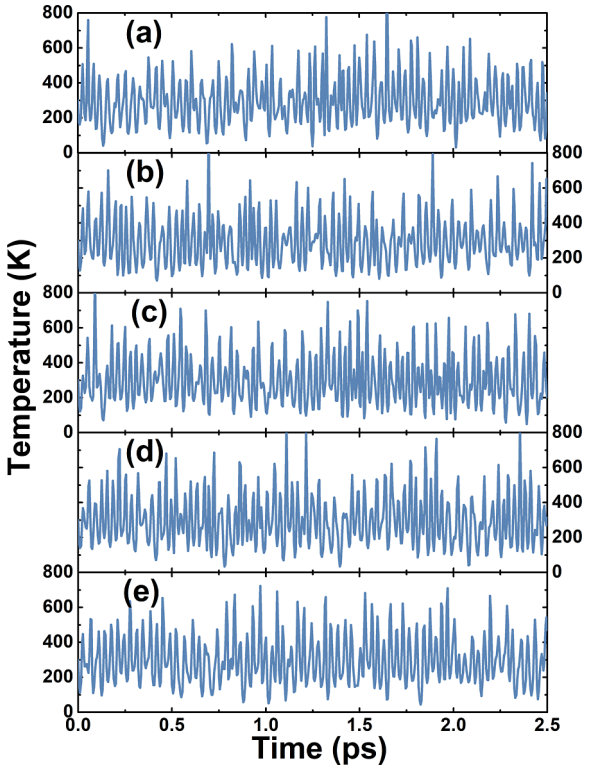

Figure 5. Fluctuation of temperature as a function of molecular dynamics simulation steps at 300 K of Cr_2N monolayer at (a) biaxial compression of −5%, (b) biaxial tension of +5%, (c) unstrained state, (d) uniaxial compression of −5%, and (e) uniaxial compression of +5%.

Regarding the magnetic properties, Figure 6a,b shows the different magnetic configuration of the 2D unstrained Cr_2N MXene and the magnetic anisotropy at the high symmetry hexagonal lattice, respectively. The Cr atoms at different polarizations are marked with yellow and red balls for spin up and spin down, respectively. The FM and different AFM configurations were considered in the calculations. Since the Cr_2N has two Cr monolayers on top and bottom, the spin in the different Cr layers was polarized parallel to each other (FM, AFM2, and AFM4), or the Cr layers are antiparallel (AFM1, AFM3, and AFM5).[37] The magnetic anisotropy is calculated by the spin−orbit coupling for magnetic alignments along the x- and z-axes, as shown in Figure 6b. Magnetic alignments are set without any constraint.

The relative energies per primitive cell of the FM, AFM1, AFM2, AFM3, AFM4, and AFM5 unstrained MXenes are 1.42, 0.93, 0.43, 0, 5.76×10^{-5}, and 0.43 eV, respectively. Note that Cr_2N unstrained has an AFM3 ground state, as described in previous reports,[37] also we consider different values of U to treat the highly correlated electrons from Cr, and our results show that $U = 3$ eV reproduces the results previously published (for more details, see Table S1 of Supporting Information). Table 3 summarizes the relative energies for the six magnetic configurations when applying compressive and tensile strain. For biaxial strain, the AFM4 is the most favorable configuration under compressive deformation; nevertheless, under tensile strain in the interval $1\% < \varepsilon \leq 3\%$, the AFM3 is the most favorable, and for larger values of strain, the system switches to AFM4 as the most favorable configuration. Meanwhile for uniaxial strain, the AFM4 is the most favorable configuration under compressive deformation in the interval $-5\% < \varepsilon \leq -3\%$ and preserve the AFM3 configuration only from $-2\% < \varepsilon \leq 0\%$, although for a tensile strain, the AFM4 is the most favorable characteristic.

Moreover, from the magnetic anisotropy energy (MAE) performed for the upper and lower strain limits, the results exhibit an out-of-plane spin alignment for unstrained and under uniaxial strain. Regarding MXene under biaxial tensile strain, it preserves the same spin alignment as unstrained Cr_2N; nevertheless, under compressive strain, the in-plane alignment is the most stable. The out-of-plane alignment is 0.05 meV less stable. Table S2 of Supporting Information displays the MAE for all deformation percentages. Note that the spin orientation changes due to the increment or decrement distance between the Cr layer (see Figure S4). This effect gains importance when applying biaxial compressive strain.

With this in mind, it can be seen that the magnetic configuration depends on the Cr−N bond length. Figure 7a,b exhibits the bond distance of Cr_2N under biaxial and uniaxial strain, respectively. Three kinds of bond lengths named as Cr−N1, Cr−N4, and Cr−N2 (black, red, and green dots-lines, respectively) have been plotted that correspond with the [−210], [−120], and [110] directions, respectively. Unstrained Cr_2N MXene displays AFM3 configuration with Cr−N4 > Cr−N1 and Cr−N1, and the Cr−N1 is equal to Cr−N2. After applying compressive or tensile strain, the bond lengths display a linear decrement or increment, respectively.

Concerning with Figure 7a, when the Cr_2N is under biaxial −5% strain, the AFM4 configuration is favorable because of keeping the relation Cr−N2 > Cr−N1 > Cr−N4 where the

https://doi.org/10.1021/acsomega.2c02751
ACS Omega 2022, 7, 33884−33894

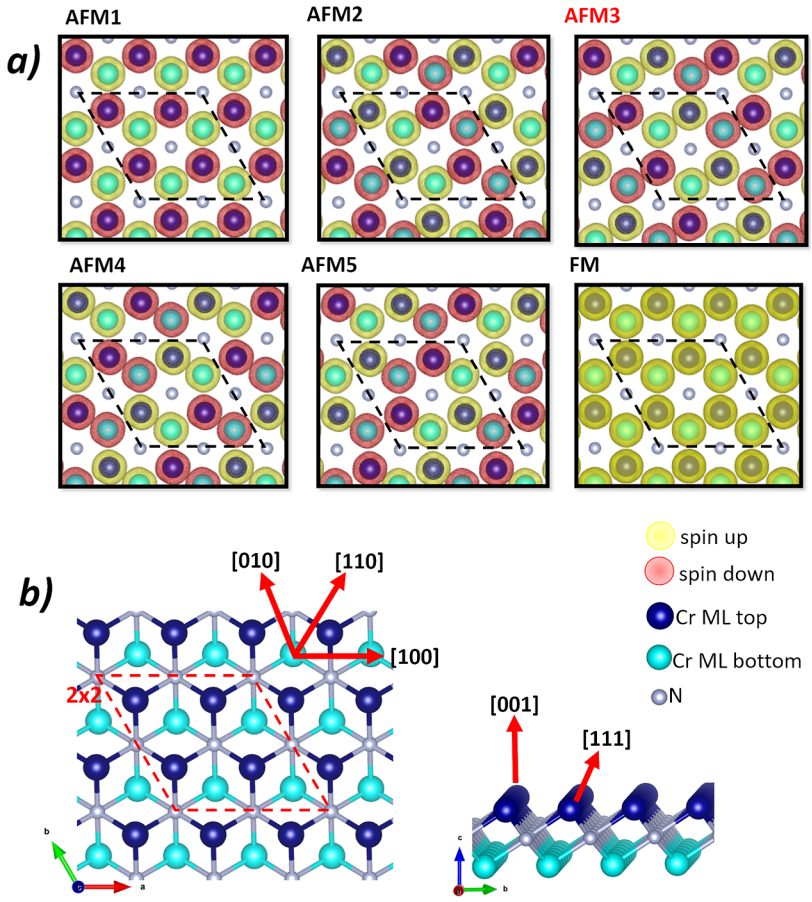

Figure 6. (a) Possible magnetic polarization in Cr_2N MXene; yellow and red balls correspond to spin up and spin down, respectively, and (b) schematic of the Cr_2N MXene structure highlighting high-symmetry axes, in-plane are (100), (110), and (010), and out-of-plane are (001) and (111) directions.

Table 3. Relative Energies (meV) of Magnetic Configurations of the Cr_2N MXene Unstrained and Biaxial and Uniaxial Strained

	biaxial strain						uniaxial strain					
% strain	FM	AFM 1	AFM 2	AFM3	AFM4	AFM 5	FM	AFM 1	AFM 2	AFM 3	AFM 4	AFM 5
−5	1783.77	1483.09	261.27	0.22	0.00	261.16	1598.39	1120.01	401.61	56.42	0.00	324.68
−4	1677.83	1332.92	288.59	0.34	0.00	288.24	1541.35	889.68	384.35	27.04	0.00	340.87
−3	1583.58	1199.23	317.49	0.03	0.00	317.19	1496.07	954.01	379.40	6.32	0.00	361.24
−2	1511.61	1089.76	349.68	0.02	0.00	349.52	1465.12	866.50	391.28	0.00	6.23	388.16
−1	1455.77	999.86	386.98	0.01	0.00	387.16	1441.17	799.23	411.30	0.00	10.91	414.51
0	1415.83	930.76	430.00	0.00	0.06	429.98	1415.83	930.76	430.00	0.00	0.06	429.98
1	1386.60	880.19	477.17	0.00	0.07	477.14	1395.83	896.76	455.05	2.71	0.00	447.24
2	1345.71	848.34	527.03	0.00	0.18	527.14	1385.53	872.73	490.91	20.52	0.00	468.43
3	1291.70	836.33	584.41	0.00	0.01	584.55	1375.33	847.45	531.54	45.00	0.00	490.50
4	1240.79	834.80	642.87	0.03	0.00	642.88	1359.91	819.48	575.53	76.33	0.00	514.32
5	1201.22	834.84	704.04	0.04	0.00	704.03	1339.38	787.40	621.93	113.01	0.00	538.98

Cr−N2 has a slope of 0.122 (green dots) and 0.105 for Cr−N1 and Cr−N4 (black and red dots, respectively). The magnetic configuration switch to AFM3 in the range from 1 to 3% strain with a relation Cr−N4 > Cr−N1 and Cr−N2; the Cr−N4 bond slope is 0.098 (red dots) and 0.107 for Cr−N2 and Cr−N1 (green and black dots, respectively), persevering the relation of Cr_2N unstrained. Although for 4 and 5% strain, the system prefers the AFM4 behavior, where Cr−N2 > Cr−N4 > Cr−N1 and the slope for Cr−N2, Cr−N1, and Cr−N4 bonds are of 0.10, 0.134, and 0.119, respectively.

In the meantime, under larger values of uniaxial compressive strain shows AFM4 due to Cr−N2 > Cr−N4 > Cr−N1 where the Cr−N2, Cr−N4, and Cr−N1 have a slope of 0.060, 0.022, and 0.071 (green, red, and black dots, respectively), see Figure 7b. Nevertheless, under −2 and −3% of compressive strain, the system switches to AFM3 configurations because the bond relations are Cr−N4 > Cr−N2 > Cr−N1 with a slope of 0.022, 0.060, and 0.071 for Cr−N4, Cr−N2, and Cr−N1, respectively (red, green, and black dots, respectively). Under tensile strain, the system has AFM4 characteristics due to Cr−N2 > Cr−N1 > Cr−N4, where Cr−N2 and Cr−N1 have a slope of 0.045

https://doi.org/10.1021/acsomega.2c02751
ACS Omega 2022, 7, 33884−33894

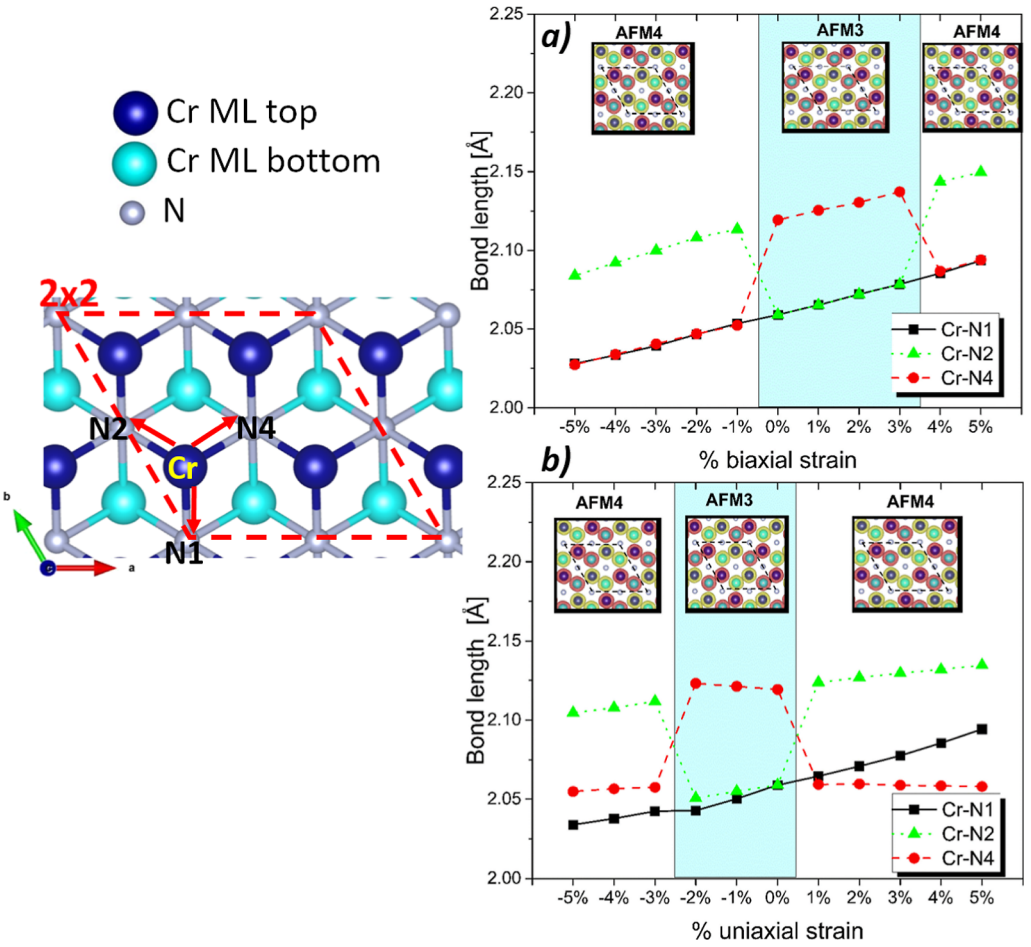

Figure 7. Bond length and the most stable magnetic configuration of the Cr_2N MXene unstrained, (a) under biaxial and (b) under uniaxial strained.

and 0.122, respectively (green and black dots, respectively) but for Cr−N4 displays a slope of 0.006 (red dots).

Regarding variation of the Cr magnetic moment magnitude, it maintains a dependence with the Cr layer distance, see Figure 8. In the other words, under biaxial and uniaxial compressive strain, the Cr magnetic moment magnitude decreases to ±3.12 μ_β and ±3.18 μ_β, respectively, in comparison with unstrained MXene ±3.23 μ_β. However, under biaxial and uniaxial tensile strain, the magnitude increases to ±3.30 μ_β and ±3.27 μ_β, respectively. It could be associated with the inverse magnetostriction effect, where the magnetic properties change after applying mechanical deformation, as shown in some 2D systems.[66−68] This could be further used to combine MXene with other 2D materials and produce VdW heterostructures.[58]

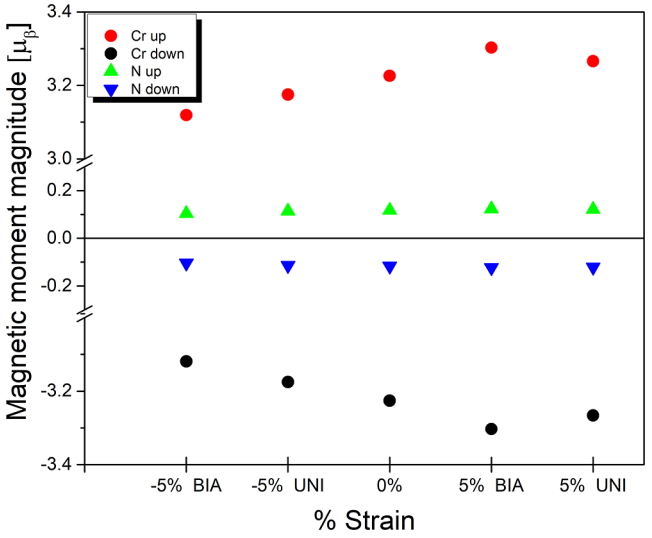

Figure 8. Cr and N magnetic moment of the Cr_2N unstrained and biaxial and uniaxial compressive/tensile strain.

Note that the magnetic moment magnitude displays a major increment or decrement when the Cr_2N is under compressive and tensile biaxial strain because the distance between Cr layer tends to be larger than that under uniaxial strain, as shown in Figure S4 of Supporting Information. Therefore, as the system is strained, the magnetic moment of Cr enhances, as shown in Cr_2NO_2.[38] Furthermore, the N atoms have induced magnetic moment either under uniaxial or biaxial strain of the order of ±0.12 μ_β.

Based on the stable magnetic configurations after applying compressive or tensile strain, the charge transfer was studied by the electron localization function (ELF) along the (001) plane. Figure 9 shows a Cr_2N MXene top view of the ELF, where the first, second, and third columns from left to right correspond to compressive strain, strain-free, and tensile strain, respectively.

ELF analysis allows a direct observation of the change of chemical bonding, the regions close to the unity (red areas)

https://doi.org/10.1021/acsomega.2c02751
ACS Omega 2022, 7, 33884−33894

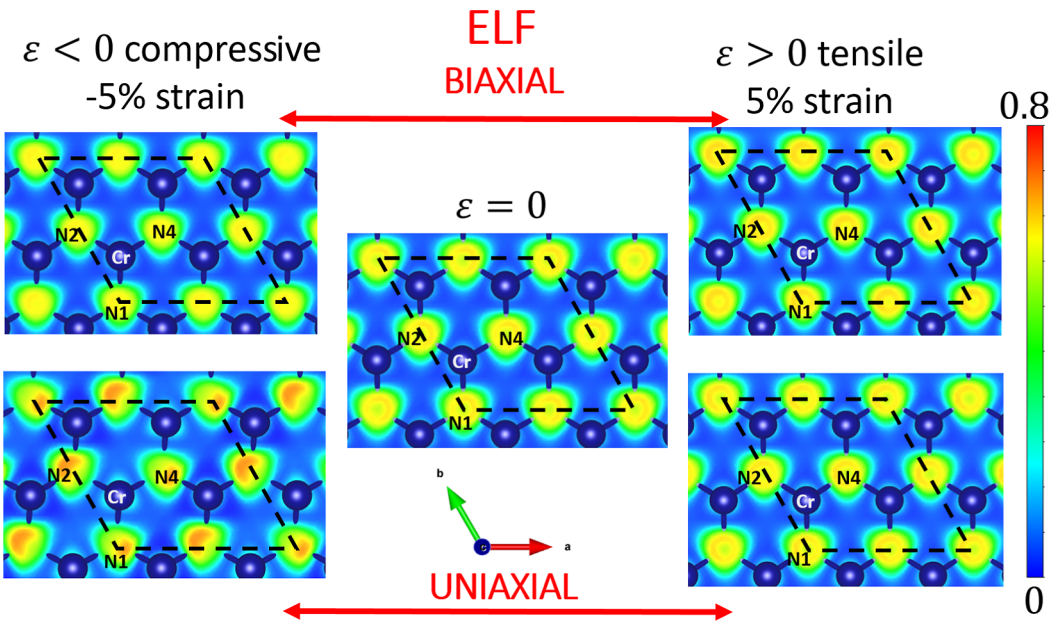

Figure 9. ELF results of the Cr_2N MXene under biaxial/uniaxial compressive strain, unstrained, and under biaxial/uniaxial tensile strain.

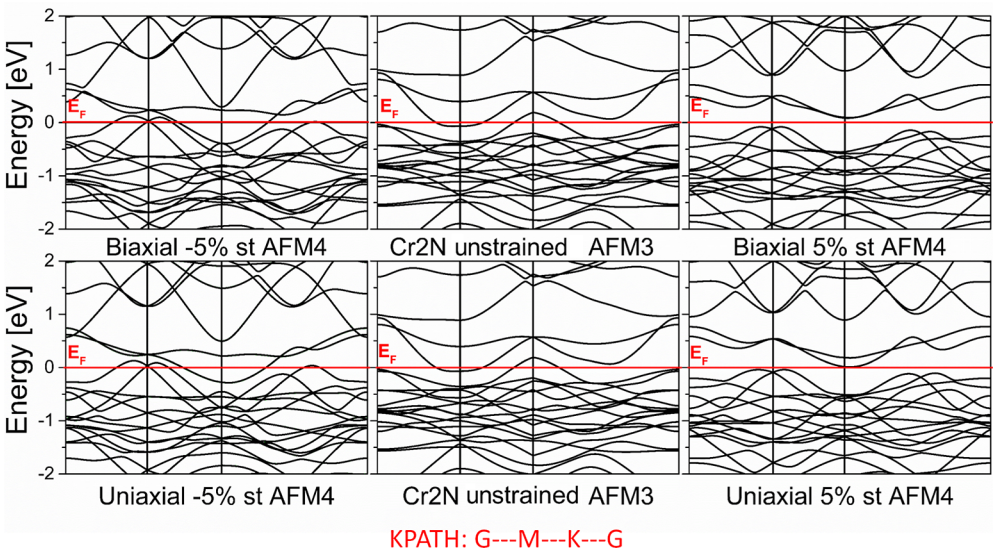

Figure 10. Band structure of MXene Cr_2N under biaxial strain, (a) compressive, (b) without strain, and (c) tensile strain. The Cr_2N with uniaxial strain, (d) compressive strain, (e) without strain, and (f) tensile strain.

contain many localized electrons, which indicates a region around a nucleus or in a very strong covalent bonding condition. Values close to zero (blue areas) represent the regions with low electron density, and the values close to 0.5 (green areas) correspond to a uniform electron gas where the bonding might have a metallic character.[69,70]

It can be noted that for unstrained Cr_2N, the Cr atom electrons are transferred to N atoms, then the electron concentration is located around N atoms, characteristics of ionic bonds.[71−73] Besides, after applying biaxial compressive strain, N atoms preserve the electron distribution. Nevertheless, under uniaxial compressive strain, the electron dispersion of N atoms is not uniform, the higher electron concentration is oriented in the direction to Cr atoms that the total electron transferred; meanwhile, the region with values close to 0.5 is oriented toward Cr atoms with a low electron density. Instead, electron clouds rise around Cr atoms that could propitiate a covalent bond with N atoms when the MXene is under biaxial and uniaxial tensile strain; this behavior is discussed with the band structure hereinafter.

To explore electronic properties, the band structure was calculated based on the stable magnetic configurations after applying compressive or tensile strain. The top and bottom graphs, as shown in Figure 10, correspond for upper and lower limits of biaxial and uniaxial strain, respectively. The compressive and tensile strain upper limits where the Cr_2N is dynamically stable in the interval from $-5\% < \varepsilon < 5\%$, strains were plotted. In all plots, the Fermi level is the energy reference. The Cr_2N MXene free-strain has a metallic behavior, which is preserved under compressive strain. Nevertheless, under tensile strain, it presents an indirect band gap, in which the valence band maximum coincides along the G-M direction and conduction band minimum locates at K-point. The band gap is of 0.16 and 0.05 eV for biaxial and uniaxial tensile strain,

https://doi.org/10.1021/acsomega.2c02751
ACS Omega 2022, 7, 33884−33894

respectively. As shown under tensile strain ELF, the increment of electron density around Cr atoms could cause a covalent bonding. Band structures for all compressive and tensile strain percentages can be found in Figures S5 and S6 in Supporting Information.

As semiconductor MXenes, where the band gap is controllable with respect to various biaxial strains,[74] the Cr_2N MXene displays a similar behavior where it preserves AFM characteristics. Note that in this case, we do not consider another band gap correction due to this behavior, which is not experimentally reported yet, we only consider the appropriate Hubbard parameter,[37,38].

CONCLUSIONS

We have performed a comprehensive study of the effect of biaxial and uniaxial stress on the structural, electronic, and magnetic properties of Cr_2N MXene through first-principles simulation. The OPG of the MXene can be continuously tuned via external compressive or tensile strain, preserving the structural stability. After applying an appropriate strain, the MXene experiments a magnetic transition from AFM3 to AFM4 configurations. The MAE displays that the unstrained MXene has an out-of-plane spin alignment and in-plane under biaxial compressive strain where the magnetic moment magnitude of the Cr atoms decreases or increases if the MXene is under compressive or tensile strain. Furthermore, the band structure graphs indicate that the MXenes under compressive strain preserve the metallic property; nevertheless, under tensile strain, it has a little indirect band gap. These properties extend the potential applications in the spintronics area as long as they can be grown on substrates with high lattice mismatch or employed with other 2D materials and produce VdW heterostructures, owing to the tunable electronic and the Cr spin orientation by the compressive or tensile strain applied.

ASSOCIATED CONTENT

Supporting Information

The Supporting Information is available free of charge at https://pubs.acs.org/doi/10.1021/acsomega.2c02751.

Parameter optimization of Cr_2N MXene free strain; phonon DOS results of Cr_2N MXene under biaxial and uniaxial strain; variation in the Cr layer distance for biaxial and uniaxial strain; optimization of the Hubbard parameter as function of the lattice parameter and magnetic moment of unstrained Cr_2N MXene; MAE of Cr_2N MXene unstrained and under deformation; and band structure of Cr_2N MXene unstrained and under deformation (PDF)

AUTHOR INFORMATION

Corresponding Authors

Sandra Julieta Gutiérrez-Ojeda − *Centro de Nanociencias y Nanotecnología, Universidad Nacional Autónoma de México, Ensenada, Baja California 22800, México;* orcid.org/0000-0002-3464-2082; Email: sjulietago@ens.cnyn.unam.mx

Ma. Guadalupe Moreno-Armenta − *Centro de Nanociencias y Nanotecnología, Universidad Nacional Autónoma de México, Ensenada, Baja California 22800, México;* Email: moreno@ens.cnyn.unam.mx

Authors

Rodrigo Ponce-Pérez − *Centro de Nanociencias y Nanotecnología, Universidad Nacional Autónoma de México, Ensenada, Baja California 22800, México;* orcid.org/0000-0002-6726-1569

Daniel Maldonado-Lopez − *Department of Chemical Engineering & Materials Science, Michigan State University, East Lansing, Michigan 48823, United States*

Do Minh Hoat − *Institute of Theoretical and Applied Research, Duy Tan University, Ha Noi 100000, Vietnam; Faculty of Natural Sciences, Duy Tan University, Da Nang 550000, Vietnam*

Jonathan Guerrero-Sánchez − *Centro de Nanociencias y Nanotecnología, Universidad Nacional Autónoma de México, Ensenada, Baja California 22800, México;* orcid.org/0000-0003-1457-9677

Complete contact information is available at: https://pubs.acs.org/10.1021/acsomega.2c02751

Notes

The authors declare no competing financial interest.

ACKNOWLEDGMENTS

We thank DGAPA-UNAM projects IA100822 and IN110820 for partial financial support. Calculations were performed in the DGCTICUNAM Supercomputing Center, projects no. LANCAD-UNAM-DGTIC-150 and LANCAD-UNAM-DGTIC-368. S.J.G.O. acknowledges DGAPA-UNAM for the postdoctoral position. J.G.S. acknowledges the THUBAT KAAL IPICYT supercomputing center for computational resources. R.P.P. acknowledges CONACYT for the postdoctoral position. The authors thankfully acknowledge the computer resources, technical expertise, and support provided by the Laboratorio Nacional de Supercomputo del Sureste de Mexico, CONACYT member of the network of national laboratories. We thank A. Rodriguez-Guerrero for technical assistance.

REFERENCES

(1) Lin, X.; Yang, W.; Wang, K. L.; Zhao, W. Two-dimensional spintronics for low-power electronics. *Nat. Electron.* **2019**, *2*, 274−283.

(2) Guo, L.; Gu, X.; Zhu, X.; Sun, X. Recent Advances in Molecular Spintronics: Multifunctional Spintronic Devices. *Adv. Mater.* **2019**, *31*, No. e1805355.

(3) Wang, K.; He, J.; Zhang, M.; Wang, H.; Zhang, G. Magnon − phonon interaction in antiferromagnetic two-dimensional MXenes. *Nanotechnology* **2020**, *31*, 435705.

(4) Geim, A. K.; Novoselov, K. S. The rise of graphene. *Nat. Mater.* **2007**, *6*, 183.

(5) Jariwala, D.; Sangwan, V. K.; Lauhon, L. J.; Marks, T. J.; Hersam, M. C. Carbon nanomaterials for electronics, optoelectronics, photovoltaics and sensing. *Chem. Soc. Rev.* **2013**, *42*, 2824−2860.

(6) Sun, M.; Luo, Y.; Yan, Y.; Schwingenschlögl, U. Ultrahigh Carrier Mobility in the Two-Dimensional Semiconductors B8Si4, B8Ge4, and B8Sn4. *Chem. Mater.* **2021**, *33*, 6475−6483.

(7) Novoselov, K. S.; Geim, A. K.; Morozov, S. V.; Jiang, D.; Zhang, Y.; Dubonos, S. V.; Grigorieva, I. V.; Firsov, A. A. Electric Field Effect in Atomically Thin Carbon Films. *Science* **2004**, *306*, 666−669.

(8) Palummo, M.; Bernardi, M.; Grossman, J. C. Exciton radiative lifetimes in two-dimensional transition metal dichalcogenides. *Nano Lett.* **2015**, *15*, 2794−2800.

(9) Sun, M.; Schwingenschlögl, U. δ-CS: A Direct-Band-Gap Semiconductor Combining Auxeticity , Ferroelasticity , and Potential for High-Efficiency Solar Cells. *Phys. Rev. Appl.* **2020**, *14*, 044015.

(10) Bafekry, A.; Karbasizadeh, S.; Faraji, M.; Khatibani, A. B.; Sarsari, I. A.; Gogova, D.; Ghergherehchi, M. Van der Waals heterostructure of graphene and gemanane: tuning the ohmic contact by electrostatic gating and mechanical strain. *Phys. Chem. Chem. Phys.* **2021**, *23*, 21196−21206.
(11) Červenka, J.; Katsnelson, M. I.; Flipse, C. F. J. Room-temperature ferromagnetism in graphite driven by two-dimensional networks of pointdefects. *Nat. Phys.* **2009**, *5*, 840−844.
(12) Lu, P.; Wu, X.; Guo, W.; Zeng, X. C. Strain-dependent electronic and magnetic properties of MoS 2 monolayer, bilayer, nanoribbons and nanotubes. *Phys. Chem. Chem. Phys.* **2012**, *14*, 13035−13040.
(13) Zhou, Y.; Wang, Z.; Yang, P.; Zu, X.; Yang, L.; Sun, X.; Gao, F. Tensile strain switched ferromagnetism in layered NbS2 and NbSe2. *ACS Nano* **2012**, *6*, 9727−9736.
(14) Zhang, S.; Li, Y.; Zhao, T.; Wang, Q. Robust ferromagnetism in monolayer chromium nitride. *Sci. Rep.* **2014**, *4*, 5241.
(15) Kuklin, A. V.; Kuzubov, A. A.; Kovaleva, E. A.; Mikhaleva, N. S.; Tomilin, F. N.; Lee, H.; Avramov, P. V. Two-dimensional hexagonal CrN with promising magnetic and optical properties: A theoretical prediction. *Nanoscale* **2017**, *9*, 621−630.
(16) Bafekry, A.; Stampfl, C.; Naseri, M.; Fadlallah, M. M.; Faraji, M.; Ghergherehchi, M.; Gogova, D.; Feghhi, S. A. H. Effect of electric field and vertical strain on the electro-optical properties of the MoSi2 N4 bilayer : A first-principles calculation Effect of electric field and vertical strain on the electro-optical properties of the MoSi 2 N 4 bilayer : A first-prin. *J. Appl. Phys.* **2021**, *129*, 155103.
(17) Yang, S.; Chen, Y. Strain engineering of two-dimensional materials : Methods , properties , and applications. *InfoMat* **2021**, *3*, 397−420.
(18) Naguib, M.; Kurtoglu, M.; Presser, V.; Lu, J.; Niu, J.; Heon, M.; Hultman, L.; Gogotsi, Y.; Barsoum, M. W. Two-Dimensional Nanocrystals Produced by Exfoliation of Ti3AlC2. *Adv. Mater.* **2011**, *23*, 4248−4253.
(19) Khazaei, M.; Arai, M.; Sasaki, T.; Chung, C.-Y.; Venkataramanan, N. S.; Estili, M.; Sakka, Y.; Kawazoe, Y. Novel electronic and magnetic properties of two-dimensional transition metal carbides and nitrides. *Adv. Funct. Mater.* **2013**, *23*, 2185−2192.
(20) Papadopoulou, K. A.; Chroneos, A.; Parfitt, D.; Christopoulos, S. R. G. A perspective on MXenes: Their synthesis, properties, and recent applications. *J. Appl. Phys.* **2020**, *128*, 170902.
(21) Gogotsi, Y.; Anasori, B. The Rise of MXenes. *ACS Nano* **2019**, *13*, 8491−8494.
(22) Khazaei, M.; Ranjbar, A.; Arai, M.; Sasaki, T.; Yunoki, S. Electronic properties and applications of MXenes: a theoretical review. *J. Mater. Chem. C* **2017**, *5*, 2488−2503.
(23) Anasori, B.; Xie, Y.; Beidaghi, M.; Lu, J.; Hosler, B. C.; Hultman, L.; Kent, P. R. C.; Gogotsi, Y.; Barsoum, M. W. Two-Dimensional, Ordered, Double Transition Metals Carbides (MXenes). *ACS Nano* **2015**, *9*, 9507−9516.
(24) Iqbal, M.; Fatheema, J.; Noor, Q.; Rani, M.; Mumtaz, M.; Zheng, R.-K.; Khan, S. A.; Rizwan, S. Co-existence of magnetic phases in two-dimensional MXene. *Mater. Today Chem.* **2020**, *16*, 100271.
(25) Gao, Q.; Zhang, H. Magnetic i-MXenes: A new class of multifunctional two-dimensional materials. *Nanoscale* **2020**, *12*, 5995−6001.
(26) Hantanasirisakul, K.; Gogotsi, Y. Electronic and Optical Properties of 2D Transition Metal Carbides and Nitrides (MXenes). *Adv. Mater.* **2018**, *30*, 1804779.
(27) Wang, J.; Zhou, X.; Yang, M.; Cao, D.; Chen, X.; Shu, H. Interface and polarization effects induced Schottky-barrier-free contacts in two-dimensional MXene/GaN heterojunctions. *J. Mater. Chem. C* **2020**, *8*, 7350−7357.
(28) Luo, L.; Huang, Y.; Cheng, K.; Alhassan, A.; Alqahtani, M.; Tang, L.; Wang, Z.; Wu, J. MXene-GaN van der Waals metal-semiconductor junctions for high performance multiple quantum well photodetectors. *Light Sci. Appl.* **2021**, *10*, 177−211.
(29) Shi, Z.; Khaledialidusti, R.; Malaki, M.; Zhang, H. MXene-based materials for solar cell applications. *Nanomaterials* **2021**, *11*, 3170.
(30) Maldonado-Lopez, D.; Rodriguez, J. R.; Pol, V. G.; Syamsai, R.; Andrews, N. G.; Gutiérrez-Ojeda, S. J.; Ponce-Pérez, R.; Moreno-Armenta, Ma G.; Guerrero-Sánchez, J. *Atomic-Scale Understanding of Li Storage Processes in the Ti4C3and Chemically Ordered Ti2Ta2C3M-Xenes: A Theoretical and Experimental Assessment*, 2021.
(31) Bafekry, A.; Akgenc, B.; Ghergherehchi, M.; Peeters, F. M. Strain and electric field tuning of semi-metallic character WCrCO 2 MXenes with dual narrow band gap. *J. Phys. Condens. Matter* **2020**, *32*, 355504.
(32) Fu, L.; Wang, X.; Mi, W. Tunable electronic structure and magnetic anisotropy of two dimensional Mn2CFCl/MoSSe van der Waals heterostructures by electric field and biaxial strain. *Appl. Surf. Sci.* **2021**, *566*, 150683.
(33) Zhong, Y.; Xia, X. H.; Shi, F.; Zhan, J. Y.; Tu, J. P.; Fan, H. J. Transition metal carbides and nitrides in energy storage and conversion. *Adv. Sci.* **2015**, *3*, 150028.
(34) Kumar, H.; Frey, N. C.; Dong, L.; Anasori, B.; Gogotsi, Y.; Shenoy, V. B. Tunable Magnetism and Transport Properties in Nitride MXenes. *ACS Nano* **2017**, *11*, 7648−7655.
(35) Morel, A.; Borjon-Piron, Y.; Porto, R. L.; Brousse, T.; Bélanger, D. Suitable Conditions for the Use of Vanadium Nitride as an Electrode for Electrochemical Capacitor. *J. Electrochem. Soc.* **2016**, *163*, A1077−A1082.
(36) Wang, D.; Gao, Y.; Liu, Y.; Jin, D.; Gogotsi, Y.; Meng, X.; Du, F.; Chen, G.; Wei, Y. First-Principles Calculations of Ti2N and Ti2NT2 (T = O, F, OH) Monolayers as Potential Anode Materials for Lithium-Ion Batteries and Beyond. *J. Phys. Chem. C* **2017**, *121*, 13025−13034.
(37) Wang, G. Theoretical Prediction of the Intrinsic Half-Metallicity in Surface-Oxygen-Passivated Cr2N MXene. *J. Phys. Chem. C* **2016**, *120*, 18850−18857.
(38) Sun, Q.; Li, J.; Li, Y.; Yang, Z.; Wu, R. Cr2NX2 MXene (X = O, F, OH): A 2D ferromagnetic half-metal. *Appl. Phys. Lett.* **2021**, *119*, 062404.
(39) Yue, Y.; Wang, B.; Miao, N.; Jiang, C.; Lu, H.; Zhang, B.; Wu, Y.; Ren, J.; Wang, M. Tuning the magnetic properties of Zr2N MXene by biaxial strain. *Ceram. Int.* **2021**, *47*, 2367−2373.
(40) Zheng, F.; Xiao, X.; Xie, J.; Zhou, L.; Li, Y.; Dong, H. Structures, properties and applications of two-dimensional metal nitrides: from nitride MXene to other metal nitrides. *2D Mater.* **2022**, *9*, 022001.
(41) Kresse, G.; Hafner, J. Norm-conserving and ultrasoft pseudopotentials for first-row and transition elements. *J. Phys. Condens. Matter* **1994**, *6*, 8245−8257.
(42) Kresse, G.; Furthmüller, J. Efficient iterative schemes for ab initio total-energy calculations using a plane-wave basis set. *Phys. Rev. B* **1996**, *54* (16), 11169−11186.
(43) Kresse, G.; Furthmüller, J. Efficiency of ab-initio total energy calculations for metals and semiconductors using a plane-wave basis set. *Comput. Mater. Sci.* **1996**, *6* (1), 15−50.
(44) Perdew, J. P.; Burke, K.; Ernzerhof, M. Generalized gradient approximation made simple. *Phys. Rev. Lett.* **1996**, *77*, 3865−3868.
(45) Anisimov, V. I.; Aryasetiawan, F.; Lichtenstein, I. First-principles calculations of the electronic structure and spectra of strongly correlated systems : the LDA + U method. *J. Phys. Condens. Matter* **1997**, *9*, 767−808.
(46) Dudarev, S.; Botton, G.; Savrasov, S. Y.; Humphreys, C. J.; Sutton, A. P. Electron-energy-loss spectra and the structural stability of nickel oxide: An LSDA+U study. *Phys. Rev. B: Condens. Matter Mater. Phys.* **1998**, *57*, 1505−1509.
(47) Ponce-Pérez, R.; Guerrero-Sanchez, J.; Gutierrez-Ojeda, S. J.; Moreno Armenta, M. G. Oxygen coverage effect on the magnetic properties of Cr2NOx (0<x<2) MXene. *ACS Appl. Electron. Mater.* **2021**, *3*, 4967−4976.
(48) Blöchl, P. E. Projector augmented-wave method. *Phys. Rev. B: Condens. Matter Mater. Phys.* **1994**, *50*, 17953.

https://doi.org/10.1021/acsomega.2c02751
ACS Omega 2022, 7, 33884−33894

(49) Kresse, G.; Joubert, D. From ultrasoft pseudopotentials to the projector augmented-wave method. *Phys. Rev. B* **1999**, *59* (3), 1758−1775.
(50) Monkhorst, H. J.; Pack, J. D. Special points for Brillouin-zone integrations. *Phys. Rev. B: Solid State* **1976**, *13*, 5188−5192.
(51) Chaput, L.; Tanaka, I.; Hug, G.; Les, V.; Cedex, N. Phonon-phonon interactions in transition metals. *Phys. Rev. B: Condens. Matter Mater. Phys.* **2011**, *84*, 094302.
(52) Togo, A.; Tanaka, I. First principles phonon calculations in materials science. *Scr. Mater.* **2015**, *108*, 1−5.
(53) Clark, S. J.; Segall, M. D.; Pickard, C. J.; Hasnip, P. J.; Probert, M. I. J.; Refson, K.; Payne, M. C. First principles methods using CASTEP. *Z. Kristallogr. Cryst. Mater.* **2005**, *220*, 567−570.
(54) Zhong, S.; Xu, B.; Cui, A.; Li, S.; Liao, S.; Wang, G.; Liu, G.; Sun, B. Robust net magnetic moment in Janus V-based Nitride MXenes: Insight from First-Principles Calculations. *ACS Omega* **2020**, *5*, 864−870.
(55) Champagne, A.; Shi, L.; Ouisse, T.; Hackens, B.; Charlier, J. C. Electronic and vibrational properties of V2 C -based MXenes: From experiments to first-principles modeling. *Phys. Rev. B* **2018**, *97*, 115439.
(56) Hu, T.; Wang, J.; Zhang, H.; Li, Z.; Hu, M.; Wang, X. Vibrational properties of Ti3C2 and Ti3C2T2 (T = O, F, OH) monosheets by first-principles calculations: A comparative study. *Phys. Chem. Chem. Phys.* **2015**, *17*, 9997−10003.
(57) Tan, Z.; Fang, Z.; Li, B.; Yang, Y. First-principles study of the ferromagnetic properties of Cr2CO2 and Cr2NO2 MXenes. *Angew. Chem., Int. Ed.* **2020**, *5*, 25848−25853.
(58) Champagne, A.; Charlier, J. C. Physical properties of 2D MXenes: From a theoretical perspective. *J. Phys. Mater.* **2020**, *3*, 032006.
(59) Yorulmaz, U.; Özden, A.; Perkgöz, N. K.; Ay, F.; Sevik, C. Vibrational and mechanical properties of single layer MXene structures: A first-principles investigation. *Nanotechnology* **2016**, *27*, 335702.
(60) Peng, B.; Zhang, H.; Shao, H.; Xu, Y.; Ni, G.; Zhang, R.; Zhu, H. Phonon transport properties of two-dimensional group-IV materials from ab initio calculations. *Phys. Rev. B* **2016**, *94*, 245420.
(61) Carrete, J.; Li, W.; Lindsay, L.; Broido, D. A.; Gallego, L. J. Physically founded phonon dispersions of few- layer materials and the case of borophene. *Mater. Res. Lett.* **2016**, *4*, 204−211.
(62) Taheri, A.; Pisana, S. Importance of quadratic dispersion in acoustic flexural phonons for thermal transport of two-dimensional materials. *Phys. Rev. B* **2021**, *103*, 235426.
(63) Kuang, Y.; Lindsay, L.; Wang, Q.; He, L. Lattice chain theories for dynamics of acoustic flexural phonons in nonpolar nanomaterials. *Phys. Rev. B* **2020**, *102*, 144301.
(64) Siriwardane, E. M. D.; Karki, P.; Loh, Y. L.; Çakır, D. Strain-Spintronics: Modulating Electronic and Magnetic Properties of Hf2MnC2O2 MXene by Uniaxial Strain. *J. Phys. Chem. C* **2019**, *123*, 12451−12459.
(65) Tohei, T.; Kuwabara, A.; Oba, F.; Tanaka, I. Debye temperature and stiffness of carbon and boron nitride polymorphs from first principles calculations. *Phys. Rev. B* **2006**, *73*, 064304.
(66) Zhao, S.; Kang, W.; Xue, J. Manipulation of electronic and magnetic properties of M 2 C (M = Hf , Nb , Sc , Ta , Ti , V , Zr) monolayer by applying mechanical strains. *Appl. Phys. Lett.* **2014**, *104*, 133106.
(67) Chen, W.; Li, H.; Shi, X.; Pan, H. Tension-Tailored Electronic and Magnetic Switching of 2D Ti 2 NO 2. *J. Phys. Chem. C* **2017**, *121*, 25729−25735.
(68) Zhao, M.; Chen, J.; Wang, S.; An, M.; Dong, S. Multiferroic properties of oxygen functionalized magnetic i-MXene. *Phys. Rev. Mater.* **2021**, *5*, 094408.
(69) Fuentealba, P.; Chamorro, E.; Santos, J. C. Understanding and using the electron localization. *Theoretical and Computational Chemistry*; Elsevier, 2007; pp 57−85.
(70) Zhang, N.; Hong, Y.; Yazdanparast, S.; Zaeem, M. A. A Comprehensive First Principles Study of Structural, Elastic and Electronic Properties of Two-Dimensional Titanium Carbide/Nitride Based MXenes. *2D Mater.* **2018**, *5*, 1−22.
(71) Guo, J.; Peng, Q.; Fu, H.; Zou, G.; Zhang, Q. Heavy-Metal Adsorption Behavior of Two-Dimensional Alkalization- Intercalated MXene by First-Principles Calculations. *J. Phys. Chem. C* **2015**, *119*, 20923−20930.
(72) Mishra, A.; Srivastava, P.; Carreras, A.; Tanaka, I.; Mizuseki, H.; Lee, K.-R.; Singh, A. K. Atomistic Origin of Phase Stability in Oxygen-Functionalized MXene. *J. Phys. Chem. C* **2017**, *121*, 18947−18953.
(73) Wang, Y.; Zhou, M.; Xu, L.; Zhao, W.; Li, R.; Yang, Z. Achieving superior high-capacity batteries with the lightest Ti 2 C MXene anode by first-principles calculations : Overarching role of S-functionate (Ti 2 CS 2) and multivalent cations carrier. *J. Power Sources* **2020**, *451*, 227791.
(74) Cui, J.; Peng, Q.; Zhou, J.; Sun, Z. Strain-tunable electronic structures and optical properties of semiconducting MXenes. *Nanotechnology* **2019**, *30*, 345205.

https://doi.org/10.1021/acsomega.2c02751
ACS Omega 2022, 7, 33884−33894